# Case Study: Visualization of Laser Confocal Microscopy Datasets

Georgios Sakas * Michael G. Vicker † Peter J. Plath ‡
Fraunhofer IGD University of Bremen University of Bremen

## Abstract

*This paper presents an example of how existing visualization methods can be successfully applied – after minor modifications – for allowing new, sometimes unexpected insight in scientific questions, in this case for better understanding unknown, microscopic biological structures. We present a volume rendering system supporting the visualization of LCM datasets, a new microscopic tomographic method allowing for the first time accurate and fast in-vivo inspection of the spatial structure of microscopic structures, especially important in (but not restricted to) biology. The speed, flexibility and versatility of the system allows fast, convenient, interactive operation with large datasets on small computers (workstation or PC). By testing different datasets we have been able to significantly improve the performance of understanding the internal structure of LCM data. Most important, we have been able to show static and dynamic structures of cells never seen before and allowing significant insight in the cell movement process. Therefore we regard our system as a universal tool for the visualization such data.*

## 1 Introduction

In recent years the efforts of the major tomographic techniques (CT, MR, PET/SPECT etc.) have been focused on the acquisition of slices from organs within the human body. The size of such organs is typically several centimeters and the resolution of the acquisition techniques has been improved down to the order of magnitude of a millimeter. After several years of research and development major advantages in both, hardware and software have been achieved and the techniques of understanding complex topologies in the macroscopic scale are now considered to be well established.

However, the structures in the microscopic scale show an even higher complexity than those of organs. As examples one can list structures of nerve cells, tissue and muscles, blood vessels etc. showing beautiful, complex, and mostly still unexplored patterns. In order to understand the spatial relationship and internal structure of such microscopic probes, tomographic series of slices are required in analogy to the tomographies used for organs and other macroscopic structures.

The first method for gathering such tomographs is based in microtomic cutting and inspection of each slice using traditional microscope methods. However, this procedure shows a long list of drawbacks: the probe must be fixed, the slices can not be arbitrarily thin, the registration of slices after cutting is very difficult and often impossible, the procedure is extremely time consuming and the probe is destroyed.

[1] Fraunhofer Institute for Computer Graphics, Wilhelminenstr. 7, 64283 Darmstadt, Germany
gsakas@igd.fhg.de, http://www.igd.fhg.de/www/igd-a7

[2] Department of Biology, Leobenerstr., 28359 Bremen, Germany vicker@zfn.uni-bremen.de

[3] Department of Chemistry, Bibliothek NW2, 28334 Bremen, Germany plath@zfn.uni-bremen.de

## 2 Principle of Laser Confocal Microscopy

Laser confocal microscopy is a relatively new method allowing for a true tomographic inspection of microscopic probes. The method operates according to a simple, basic principle [9].

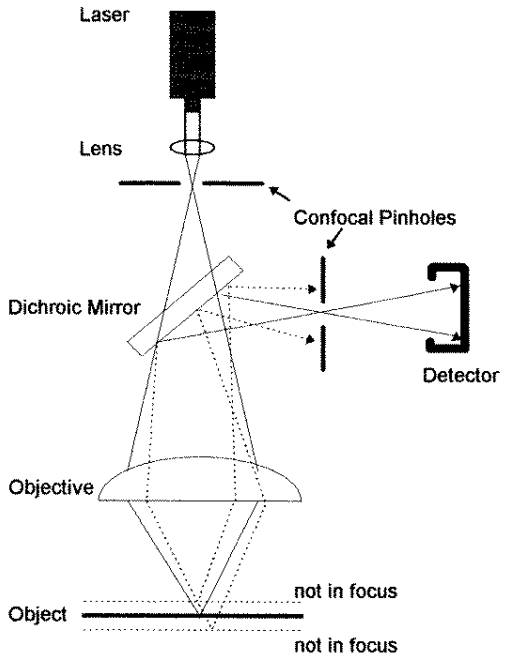


Figure 1: Principle of Laser Confocal Microscopy

Visible or ultra violet laser emission is focused on the first confocal pinhole and then onto the specimen as a diffraction-limited light spot, see fig. 1. The primary incident light is then reflected from particular voxel elements or emitted from fluorescent molecules excited within it. Emissions from the object return along the primary laser light pathway and depart from it by lateral reflection from (or passage through, depending on the instrument) a dichroic mirror onto the second confocal pinhole. This aperture is confocal with the in-focus voxel elements in the specimen. The virtual elimination by defocusing of all distal and proximal flanking emissions at this physical point assures that the light passing onto the detector, a sensitive photodetector or camera, is specifically derived from in-focus object voxels with a resolution, e.g. in the Leica instrument, approaching 200 to 400 nm in the x/y and z directions, respectively. In order to image the entire object, the light spot is scanned by a second mirror in the x/y plane in successive z sections by means of a precision stage motor. Rapid scanning preserves fluorescent intensity but must be reconciled with image quality. The storage, retrieval and manipulation of light intensity

information from the object makes static and dynamic 3-D imaging possible.
Although not perfect, the new method shows several significant benefits as compared to the traditional procedures. The most important of them are: true tomographic method, significant freedom in choosing slice thickness and size, trivial registration of slices, very fast and easy in operation, capable of acquiring in-vivo cells as well as static or dynamic structures, non-destructive. Lastly, by using different types of laser and fluorophore materials, different spatially overlapping structures can be visualized and superimposed within the same probe.

# 3 The Visualization Problems

The data acquired with Laser Confocal Microscopy (LCM) show several characteristics requiring specialized treatment in order to make the method applicable:

1. Large data size. Typical datasets have a resolution of $512^2 \times 64$ pixels. These pixels are colored, thus a typical RGB dataset requires some 50 Mbytes of memory. Obviously, datasets of this size require efficient processing methods.
2. Low contrast, low intensity gradients, bad signal to noise ratio. These characteristics make a straight-forward segmentation between the structures of interest and the background (e.g. by using thresholding, region growing, homogeneity, color differences etc.) impossible. All the methods listed above apply more or less binary decision criteria if a pixel/voxel belongs to the structure or not. Such criteria typically fail when used with signals showing the characteristics listed above.
3. Unequal resolutions in the plane and the depth directions. Thus, a visualization method has to be able to perform with "blocks" or unequal size lengths instead with cubic voxels. Re-sampling of the raw data to a regular cubic field will further reduce the signal quality, introduce interpolation artifacts and generate an even larger dataset, probably too large to be handled with conventional computers.
4. In general the examined structured is unknown. This has several implications on the quality and the speed of the visualization method:
   - Regarding the quality, artifacts have to be avoided as far as possible. Introducing artifacts in an unknown structure will often have fatal effects on their interpretation, since the human observer does not always have the experience for judging the correctness or the fidelity of the presented structures. As an example, an obvious artifact caused by bas parameter settings of the software during the visualization of human anatomy (e.g. of a head) is immediately detected by the observer, since the human anatomy is well known and such artifacts are trivially detected. This is not the case when inspecting an unknown dataset.
   - Choosing the "correct" illumination model (e.g. MIP, semi-transparent, surface etc.) has a significant impact on the clarity and information content of the visualization. Again, due to the lack of experience such a decision is typically much more difficulty than in the case of anatomic tomographic data.
   - The speed of visualization becomes the most crucial issue. The visualization parameters have to be adjusted in an interactive, trial-and-error procedure. This can take a very long time if, e.g., after an adjustment the user has to wait for several minutes to see the new result. Furthermore, inspection of new, unknown structures require rapid changing of directions, illumination conditions, visualization models, etc.. Looping and stereo images are of enormous importance for understanding unknown, complicated spatial structures.

# 4 Volume Rendering LCM Data

The term "volume rendering" refers to techniques for direct visualizing measured or simulated, discrete or continuous, scalar or vector data distributed over 3-D space, i.e., without mapping the data on intermediate representations [4], [5]. [1]. Volume rendering is the method of choice for visualizing LCM fields since it works directly on the raw data without requiring a pre-processing or segmentation step introducing artifacts. Furthermore, all parameters of visualization can be adjusted on-the-fly at will.

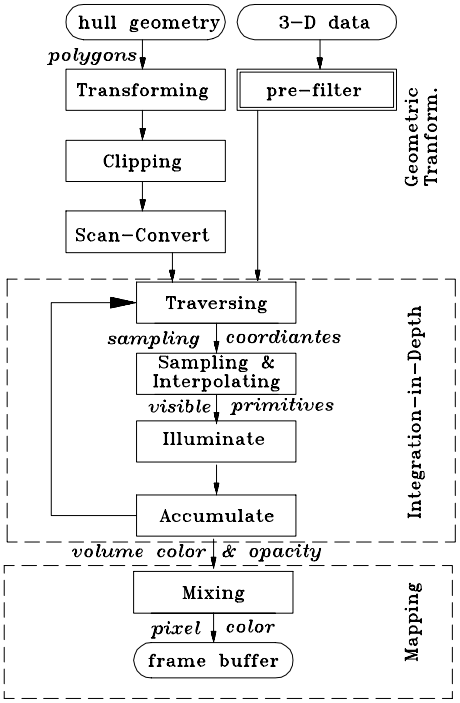


Figure 2: *The visualization pipeline.*

Volume rendering is a long established, well understood research topic for a rather long period of time, and a rich literature exists here. Therefore in this Case Study we skip most of the technical details and focusing on the application of using volume rendering for LCM data visualization. For the shake of competence we only resume the very basic milestones of volume rendering. For more details the interested reader can refer the original literature (e.g. [1]).
The visualization pipeline consists of three stages, as presented in fig. 2 [6], [7]. The 3D data are initially represented as a cube. During the "geometric transformation" stage the data are transformed, (perspectively) projected, and scan-converted using usual scanline techniques before the visible portion is clipped. In the "traversing" step the volume data are traversed using a ray-marching scheme similar to the well-known ray tracing. Different methods (e.g. splatting, shear-warp etc.) are also possible. During traversing the densities along the eye-ray are "sampled", i.e. properly weighted and accumulated. In the next "illumination" stage mapping of the data to visible primitives is performed. The three most frequently used techniques in volume rendering include (a) the reconstruction of the appearance of surfaces, used widely for the visualization of medical data like CT or MRI [4], [5] (b) the maximum or minimum intensity projection (MIP), [8] or (c) the visualization as semi-transparent gels having frequently the appearance of clouds or X-rays [4]. Each of these representations possesses advantages when used with particular types of data. The result

of this stage is an RGB-color and transparency stored in the frame buffer. Before the picture is displayed, 2-D image processing ("imaging") may be applied on the frame buffer.

# 5 Implementation and Results

For the visualization of LCM data we used our volume rendering system InViVo (**In**teractive **Vi**sualizer of **Vo**lume data) [7]. The system fulfills all requirements listed above: flexible configuration, on-the-fly adjustment of all visualization parameters, all tree types of illumination models (surface, MIP, cloud), loops and stereo, etc. In addition InViVo is implemented exclusively in software and requires no special capabilities such as graphics engine, special boards or processor types etc.. As a result InViVo runs machine-independent and is available on all types of computers running UNIX/Linux and X/Motif (supercomputers, workstations, PC etc.). Please see **http://www.igd.fhg.de/www/igd-a7/invivo.html** for detailed information about the current InViVo features. The most important feature of InViVo lies in its unmatched performance. Due to significant optimization efforts, the visualization of typical LCM datasets requires only a few seconds using a Pentium PC or PowerPC processor. Typical workstations are usually somehow slower, an effect resulting from the fact that the software implementation of InViVo requires only processor performance and tact-rate, therefore other capabilities of workstations (e.g. faster networking, graphics engines etc.) are not employed. Last, InViVo is parallelized in both, shared memory (SGI, SUN) as well as distributed memory architectures (Parsytec) showing an almost linear speed-up with increasing number of processors. In the following table the runtimes for several datasets are given.

| Data Resolution | Processor Type | | | |
|---|---|---|---|---|
| | Sparc20 | SGI | 586 | PowerPC |
| $335 \cdot 306 \cdot 67$ | 2.5 | 2.4 | 1.8 | 1.0 |
| $512^2 \cdot 100$ | 13.2 | 12.1 | 9.3 | 5.2 |
| $512 \cdot 484 \cdot 43$ | 3.6 | 3.4 | 2.5 | 1.5 |
| $512 \cdot 484 \cdot 70$ | 6.4 | 6.1 | 4.5 | 2.6 |

Table 1: *Runtimes in CPU seconds for visualizing the datasets of varying resolution presented in the paper on different computers. The image resolution is* $256^2$*, the illumination model is MIP.*

## 5.1 Visualization of Static Probes

Under the term "static" we understand microscopic structures which in general do not change shape rapidly as compared to the observation time. Typical examples of static structures are cells, bones, muscles etc. etc. In general the vast majority of microscopic probes can be considered as to be static structures. An important reason for this is that preparation and observation of rapidly changing, dynamic structures, shows usually significantly difficulties.

Figures 8 and 7 present a microscopic preparation of the tubular structure of a cat retina. The used microscope was able to detect two different fluorophore types separately, thus acquiring two different tissue types simultaneously. The dataset consist of $335 \times 306 \times 67$ voxels, each with a dimension of $0.16^2 \times 0.2 \mu m$. The first image presents the extra-cellular component of the blood vessel. The vessel diameter before the branch point is 19 $\mu m$. The second image shows the wire-like structure of the astrocyte cytosceleton. Both datasets originate from the same probe. In all subsequent images the difference of the visualization between slicing, MIP, surface and semi-transparent methods is shown.

The next dataset 6 shows the complicated structure of nerve cells networks. The resolution of the dataset is with 25 Mbytes ($512^2 \times 100$ voxels) large. As one can see on image 6 upper left, single slices are not able to provide full understanding of the complicated topology. The three other images show in much better detail the internal structure of the cell network.

## 5.2 Visualization of Dynamic Cell Structures

Laser confocal microscopy plays a fundamental role for gathering in-vivo data about not only static, but also dynamic structures, i.e. structures existing typically only within living cells and for a very short period of time (e.g. for a few seconds.). Such structures are common in several biological applications. In the case studied here we focus on temporary structures formed by polymerized actin, a structure necessary for cell movements.

For locomotion cells like *Dictyostelium* amoebae (see fig 5) forms pseudopodia by changing their shape. The changes in the cell shape are caused by the polymerization of actin. In contrast to monomeric G-actin, polymeric (filamentous) F-actin can be "colored" with fluorescence makers [2]. In this way the dynamics of the formation of short living polymerization structures can be detected. The complex dynamic of the three-dimensional periphery can be studied by means of LCM data visualization. Analyzing the temporal changes of the three-dimensional cell periphery - for example by the Karhunen-Loeve method [3]- allow us to estimate the essential data for the cell mobility. This will enable us to classify possible cell decreases by means of the cell mobility. This is important not only for *Dictyostelium* amoebae. but for all cells, which move around, for example white blood cells. Furthermore, the formation of the pseudopodia is strongly correlated with the structure formation during the polymerization of actin inside the cell. There are complex three-dimensional structures like spiral and scroll waves, which can be realized for short periods of time. By means of LCM visualization such structures can be studied in detail. The "life-time" of the different temporary structures inside the cells will give another possibility to classify .deseasethological conditions at the cellular level

Figures 3, 4 and 5 demonstrate the importance of LCM data visualization for detecting unknown structures. In this case, we studied actin filaments in *Dictyostelium* amoebae. This cell is a model of phagocytosis and chemotaxis, behaving much like the neutrophil leukocytes in our own blood. It also passes through a developmental phase in which about 100,000 cells aggregate and differentiate into 3 or 4 cell types which form a little slug that may crawl off to sporulate, partly modeling our own development. New research using this cell has shown that, contrary to earlier assumptions, **cell movement in amoeboid cells is not a random process**. To describe the pericellular spatio-temporal extension of pseudopodia which drive the locomotion of these cells one normally thinks of the incoherence movement of a sack containing 5 playful kittens. But upon closer inspection, the cell surface decomposes into the oscillating product of superimposed, rotating waves [2], [3]. The origin of these waves lies in the highly dynamic assembly and disassembly of actin proteins into short filaments in alternate corners of the cell with time periods ranging from 10 to 100 s.

All 3 figures show fluorescently stained actin filaments (F-actin) building larger patterns in fixed cells. The structure and dynamics of these patterns have not yet been studied in detail. F-actin appears to assemble into small structures or, at other intervals, more evenly as a cortex under the cell surface membrane, as in figs. 3 and 4. Here, F-actin molds the cell surface into an highly irregular pattern. This particular type of pattern is not revealed by using any other visualization method (slices, MIP or transmission ray). Fig. 3 shows F-actin structures with a size aof about 10-20 micrometers The data resolution is $512 \times 484 \times 43$ voxels = 10 Mbytes. Note the structure of the surface visible in the "surface vol-

ume rendering" image. Fig. 4 shows similar structures from a different cell. Note that the surface of the actin block is not flat but shows a complicated structure with several spikes and "antenas" (pseudopodia). These structures are hardly visible and therefore difficult to detect when regarding individual slices. Fig. 5 shows close-ups of the structure in an active pseudopodium in the upper-left hand corner of one slice, i.e., a "pretzel-like" pattern. Close examination indicates a wavefront of F-actin filament assembly. By using the volumetric methods presented here, a complete investigation of this structure (rotation, measurement, volumetry, etc.) could be produced.

## 6 Conclusion

We presented a volume rendering method supporting the visualization of LCM datasets. The speed and versatility of our implementation allows for a convenient, fast, interactive examination of unknown cell structures even on small, of-the-self computer such as PC or PowerPC. By testing different datasets we have been able to significantly improve the task of understanding the internal structure of LCM data. In addition to the static images we have been able to also visualize dynamically changing temporary structures of polymerized actin. Furthermore, for the first time we have been able to present the complicated surface of such structures, allowing insight in a process of great biological importance not completely understood yet.


## Acknowledgments

Thanks to H.T.M. van der Voort, Department of Molecular Biology, University of Amsterdam for the data of figures 8 and 7, and to Herbert Stüttler and Martin Hoppe, Leica Lasertechnik GmbH for the data of image 6.


## References


[1] Kaufman, A. (Ed.): *Volume Visualization*, IEEE Computer Society Press Tutorial, Los Alamitos/CA, 1990

[2] Killich, T.; Plath, P.J.; Xiang, W.; Bultmann, H.; Rensing, L.,Vicker, M.G.: *The locomotion, shape and pseudopodial dynamics of unstimulated Dictyostelium cells are not random*, Journal of Cell Science, 106, 1005-1013, 1993

[3] Killich, T.; Plath, P.J.; Hass, E.-C.; Xiang, W.; Bultmann, H.; Rensing, L., Vicker, M.G.: *Cell movement and shape are non-random and determined by intracellular, oscillatory, rotating waves in Dictyostelium amoebae*, BioSystems 33, 75-87, 1994

[4] Levoy, M.: *Display of Surfaces from Volume Data*, IEEE Computer Graphics & Applications, Vol. 8, No. 3, pp. 29-37, May 1988

[5] Levoy, M.: *Efficient Ray-Tracing of Volume Data*, ACM Transactions on Graphics, Vol. 9, No. 3, pp. 245-261, July 1990

[6] Sakas, G., Hartig, J.: *Interactive Visualization of Large Scalar Voxel Fields*, Proceedings IEEE Visualization'92 conference, pp. 29-36, Boston-MA, 19-22 October 1992

[7] Sakas, G.: *Interactive Volume Rendering of Large Fields*, "The Visual Computer", Vol. 9, No. 8, pp. 425-438, August 1993

[8] Sakas, G., Grimm, M., Savopoulos, A.: *Optimized Maximum Intensity Projection (MIP)*, P. Hanrahan, W. Purgathofer (Eds.) "Rendering Techniques '95", Springer Verlag Wien/New York, pp. 51-63, 1995

[9] Shotton D.M.: *Confocal scanning optical microscopy and its applications for biological specimens*, Journal of Cell Science, 94, 175-206, 1989


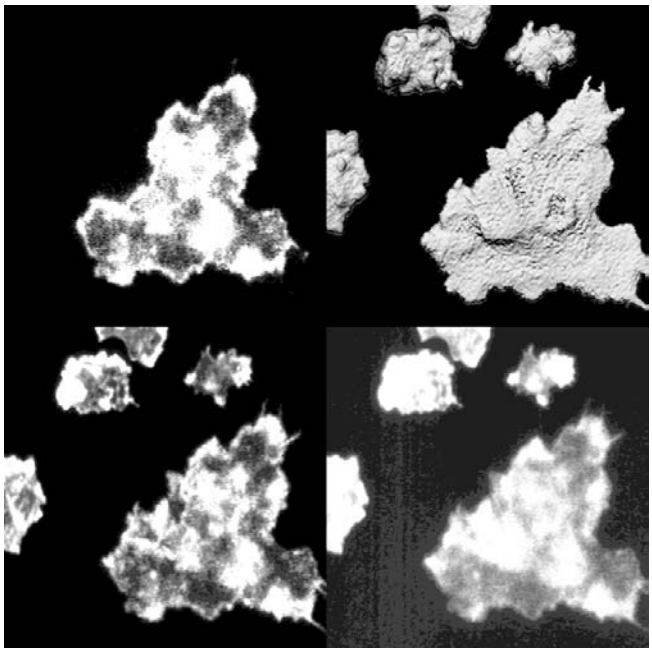

Figure 3: F-actin structures in *Dictyostelium amoebae*, Resolution $512 \times 484 \times 43$ voxels = 10 Mbytes. Upper left a single slice, right surface reconstruction; lower left MIP, right transmission illumination models

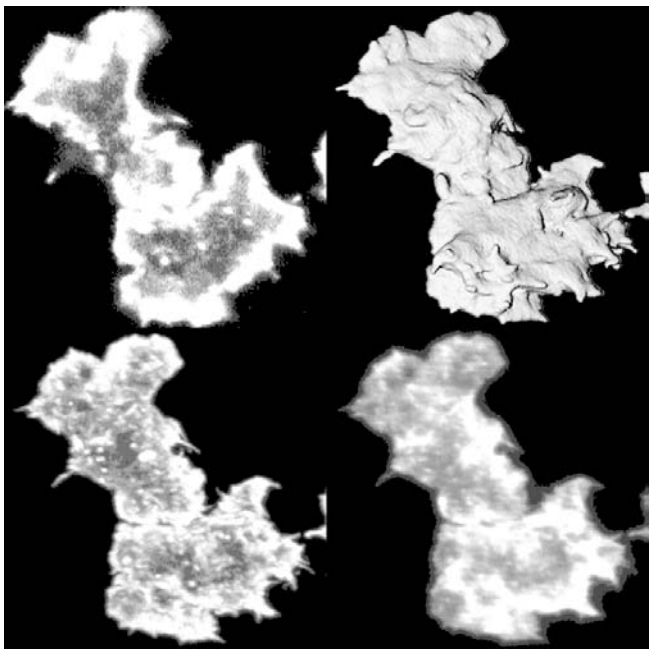

Figure 4: F-actin structures. Resolution $512 \times 484 \times 70$ voxels = 16.5 Mbytes. Upper left a single slice, right surface reconstruction; lower left MIP, right transmission illumination models

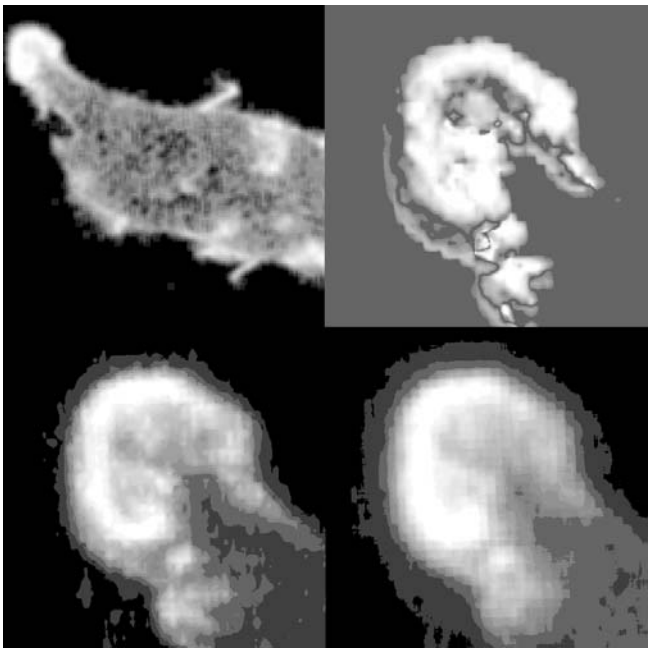

Figure 5: Close inspection of a "pretzel-like" structure located in the upper left area (pseudopodium) of the slice. Total dataset resolution $512 \times 484 \times 60$ voxels = 14 Mbytes

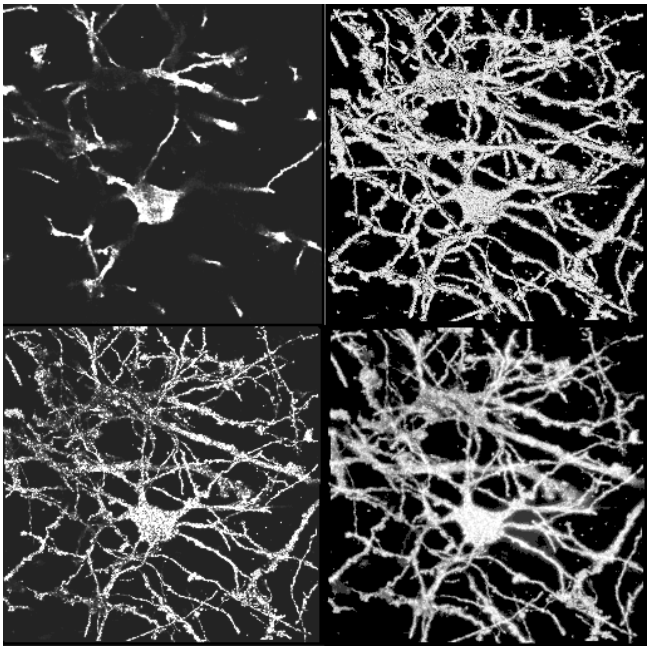

Figure 6: The complicated topology of nerve cells networks. Resolution $512^2 x100$ voxels = 25 MBytes. Upper left a single slice, right surface reconstruction; lower left MIP, right transmission illumination models

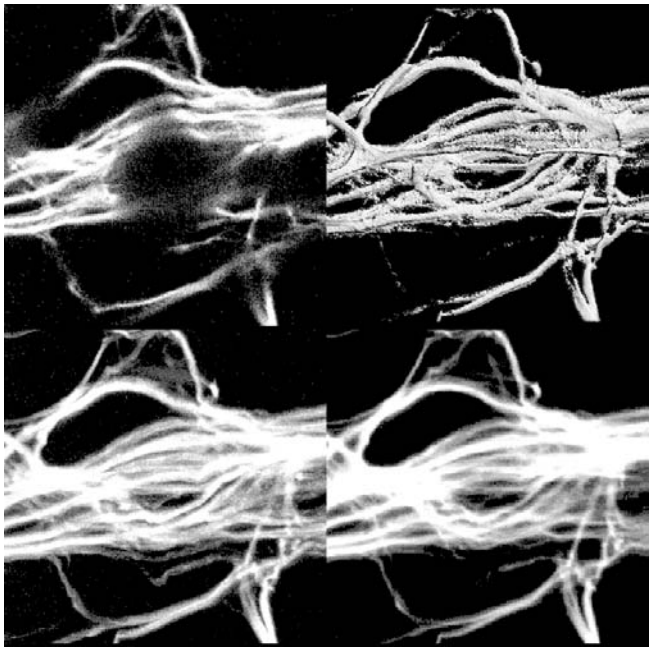

Figure 7: The wire-like structure of the astrocyte cytosceleton of the same probe. Resolution of $335 \times 306 \times 67$ voxels with a size of $0.16^2 \times 0.2 \mu m$. Upper left a single slice, right surface reconstruction; lower left MIP, right transmission illumination models

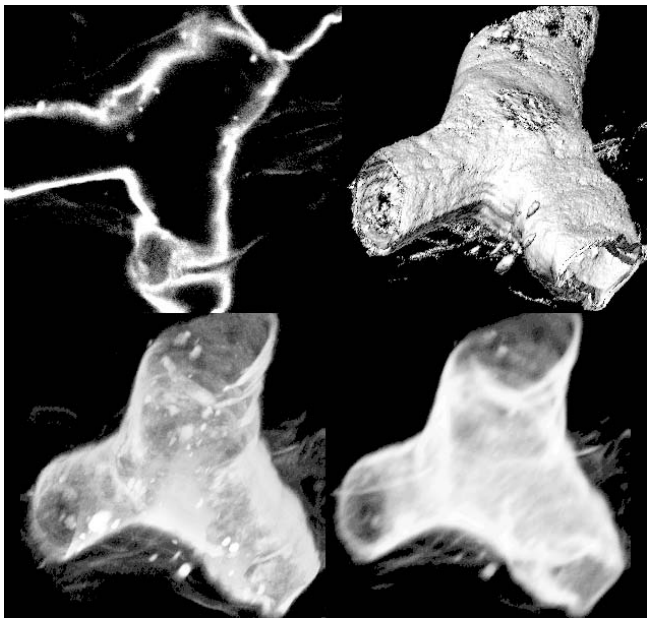

Figure 8: The extra-cellular component of a retina blood vessel of a cat. Resolution of $335 \times 306 \times 67$ voxels with a size of $0.16^2 \times 0.2 \mu m$. Upper left a single slice, right surface reconstruction; lower left MIP, right transmission illumination models